A simple approach to balancing conductivity and capacity fade in vanadium redox flow batteries by the tunable pretreatment of polybenzimidazole membranes

Journal Article

Author(s):
Hampson, Elizabeth; Duburg, Jacobus C.; Casella, Joel; Schmidt, Thomas; Gubler, Lorenz

Publication date:
2024-04-01

Permanent link:
https://doi.org/10.3929/ethz-b-000666210

Originally published in:
Chemical Engineering Journal 485, https://doi.org/10.1016/j.cej.2024.149930

Chemical Engineering Journal 485 (2024) 149930

Contents lists available at ScienceDirect

Chemical Engineering Journal

journal homepage: www.elsevier.com/locate/cej

A simple approach to balancing conductivity and capacity fade in vanadium redox flow batteries by the tunable pretreatment of polybenzimidazole membranes

Elizabeth Hampson [a,1,2], Jacobus C. Duburg [a,1], Joel Casella [a], Thomas J. Schmidt [a,b], Lorenz Gubler [a,*]

[a] Electrochemistry Laboratory, Paul Scherrer Institute, CH-5232 Villigen PSI, Switzerland
[b] Institute of Molecular Physical Science, ETH Zurich, CH-8093 Zurich, Switzerland

ARTICLE INFO

Keywords:
Polybenzimidazole
Redox flow battery
Membrane
Conductivity
Capacity

ABSTRACT

The membrane, a critical component of a vanadium redox flow battery (VRFB) cell, largely governs the battery performance through its barrier properties and ohmic resistance, as well as contributes substantially to cell stack cost in commercial systems. Polybenzimidazole (PBI) is emerging as a promising commercially available material for VRFB membranes with properties that can be tailored through suitable low-cost pretreatments. Herein, we demonstrate how pre-swelling in blended alkaline solutions can be a highly effective and accessible strategy to improve PBI conductivity for application as a VRFB membrane, whilst enabling the tunable balancing of trade–off relations with electrolyte crossover that lead to undesirable capacity fade. A figure of merit is determined, showing that the inclusion of fractions of both NaOH and KOH in the pretreatment mixture is deemed necessary to ensure that both vanadium permeability and area-specific resistance are sufficiently minimized, respectively, in the membrane by achieving optimal, intermediate levels of swelling. By applying blended pretreatments, PBI membranes could be tailored to result in high performance cell tests, exhibiting stable and high energy efficiencies of ~85 % with minimal capacity fade over 100 cycles at 120 mA·cm^{-2}.

1. Introduction

Vanadium redox flow batteries (VRFBs) offer the prospect of long-term stationary electricity storage, but are challenged with the need to reduce high capital and operational costs in order to achieve wider commercial viability [1–4]. The use of materials that are low-cost, durable and high-performance, in that maximized and maintained battery efficiencies can be achieved, is key to addressing this. As such, the membrane is a critical component in that it governs the transport and balance of electrolyte within a cell that can instigate capacity losses, as well as largely influences resistance and coulombic losses [5], all of which determine long-term cell performance and overall efficiency. Perfluorinated ion exchange membranes, particularly those of the Nafion™ series, employed industrially as the benchmark materials for VRFB membranes benefit from excellent conductivity and high chemical stability [6,7]. However, their wide application is disadvantaged by their high material and manufacturing costs, particularly in consideration of their shortcomings in performance [8,9]. Furthermore, growing concerns about the environmental and health impacts of the production and use of per- and polyfluoroalkyl substances (PFSAs) and their emerging regulations threaten the future availability of this material class [10,11]. As cation exchange membranes (CEMs) they are highly prone to vanadium ion crossover, compromising cycling stability and capacity retention which causes the necessity for deploying maintenance strategies such as electrolyte rebalancing which instigate further operating expenses [12,13].

Emerging as an attractive alternative material for VRFB applications, polybenzimidazole (PBI) is a heterocyclic polymer that exhibits excellent thermochemical and mechanical stability whilst bearing a cheaper production cost than the commercially benchmark materials discussed [14]. In the acidic nature of a typical vanadium electrolyte (1–2 M vanadium in 2–4 M H_2SO_4), the benzimidazole groups in the polymer are

* Corresponding author.
E-mail address: Lorenz.Gubler@psi.ch (L. Gubler).
[1] These authors contributed equally to this work.
[2] Current Address: Chemspeed Technologies AG, 4414 Füllinsdorf, Switzerland.

https://doi.org/10.1016/j.cej.2024.149930
Received 22 December 2023; Received in revised form 9 February 2024; Accepted 21 February 2024
Available online 22 February 2024

protonated, promoting conductivity through proton transfer via hydrogen bonding with electrolyte ions and water and rendering the PBI material an anion exchange membrane (AEM) [15,16]. In comparison to CEMs, this favorably results in low vanadium ion permeability through the Donnan exclusion effect and reduced capacity fading consequential of electrolyte crossover [17]. Unfortunately, the dense chain packing structure of PBI causes the material to be afflicted by intrinsically low proton conductivity, leading to susceptibility of high ohmic losses when used as a cell membrane. A variety of approaches can be taken to prepare PBI-based membranes with enhanced conductivity and barrier properties, including: chemical modification of the PBI backbone [18,19], blending of PBI with polymers with higher conductivity [20], using very thin (≤7 μm) PBI layers that are supported in composite membrane systems [21,22], and employing fabrication methods to controllably create sponge-like pores or voids in the material [14,23,24]. Additionally, a more accessible material processing approach can be taken, in which solution pretreatments can be applied to the membrane before cell assembly that induces swelling in the material. This causes expansion of the dense chain packing structure of PBI, creating a greater free volume that allows for a higher acid and water content and enhanced ionic pathways for conduction. The pre-swelling of PBI in high concentrations of phosphoric (~15 M) or sulfuric acid (10–12 M) has been shown to increase its proton conductivity in sulfuric acid by approximately 4 times [25]. However, balancing the benefit of increased conductivity with the subsequent increase in vanadium permeability through swelling proves to remain challenging [26].

In contrast to acid doping, studies on the effects of alkali doping on the swelling and properties of PBI membranes are far fewer, and are mostly limited to the context of fuel cell or electrolyzer applications [27–29]. The material properties and membrane qualities have been shown to be dependent on base composition, concentration, temperature and immersion time and, therefore, should be tailorable through controlled treatment and uptake [27,30]. In a recent study, Henkensmeier and co-workers demonstrated that the pre–swelling of PBI in 4 M NaOH or 4 M KOH solutions before equilibration in sulfuric acid could lower its area specific resistance (ASR) by 3–7 times [31]. However, it is clear that further understanding of the degrees of swelling accessible by alkaline hydroxides and the subsequent effects on the membrane properties, and treatment optimization is necessary to effectively utilize this pretreatment approach.

Herein, we report the preparation of poly(2,2′(*meta*-phenylene)-5,5′-bibenzimidazole) (*m*-PBI) membranes and explore the use of alkaline hydroxide pretreatments, including mixed compositions, to tune their material properties. The effects of the modified membrane characteristics on the performance of a VRFB cell are then evaluated in cycling tests, with the aim to identify the optimized pretreatment presented by a figure of merit describing capacity retention in relation to membrane ohmic resistance.

2. Experimental methods

2.1. Materials

All chemicals and materials were used as purchased from the supplier without purification unless stated. *meta*–Polybenzimidazole (*m*-PBI) with a dry thickness of 55 μm was supplied by BASF. Nafion™ NR212 was obtained from Ion Power and was soaked in 2 M H_2SO_4 for 24 h before characterization or use in cell tests. The following hydroxides were used: lithium hydroxide (98+%, Sigma-Aldrich), sodium hydroxide (pellets, ≥98 %, Sigma-Aldrich), potassium hydroxide (pellets, SLR, Fisher Scientific), rubidium hydroxide solution (50 wt% in H_2O, 99.9 %, Sigma-Aldrich), cesium hydroxide solution (50 wt% in H_2O, 99 %, Sigma-Aldrich), cesium hydroxide hydrate (99.9 % Cs, abcr swiss AG). 2 M and 4 M hydroxide solutions were prepared by dissolving or diluting the hydroxide as bought in distilled water. Na-/K-OH blended pretreatment solutions were prepared by mixing 4 M solutions of NaOH and KOH in 1:1 or 1:3 volumetric ratios. 2 M H_2SO_4 solutions were prepared from concentrated sulfuric acid (95–98 %, ACS, Sigma-Aldrich) diluted with distilled water. *N*,*N*-dimethylacetamide (DMAc) (ReagentPlus®, ≥99 %, Sigma-Aldrich) was dried over molecular sieves before use. The vanadium electrolyte was obtained commercially (Oxkem, Reading, UK) and consists of a solution of $VOSO_4$ and $V_2(SO_4)_3$ (1:1) in 2 M H_2SO_4 and 0.05 M H_3PO_4. The exact molarity of the specific batch of electrolyte used in this work (1.694 M) was determined by ICP-OES and was used for all calculations.

2.2. Methods

All procedures and experiments were conducted at room temperature unless stated otherwise.

2.2.1. Membrane preparation

m-PBI film (55 μm dry thickness) was cut into small pieces and dissolved overnight in dry DMAc at 60 °C to prepare a 15 wt% solution. After cooling to RT, the solution was filtered through a 3.1 μm syringe filter. The solution was then cast at room temperature onto a clean glass plate using a doctor blade apparatus (Zehnter ZAA 2600) with a fixed applicator gap and a speed of 7 mm·s^{-1}. Films were cast at an approximate size of 80 x 200 mm. The glass plates were immediately placed into a convection oven at 140 °C and dried for 3 h. After cooling to RT in air, the average dry thickness of the membranes on the plates was determined at a minimal of four positions using a profilometer (Dektak 8 Advanced Development Profiler, Veeco, United States). Average dry thicknesses of 14.5 μm and 35 μm were measured for the *m*-PBI membranes cast with this methodology using a 200 μm and 500 μm blade gap, respectively. The membranes were removed from the glass plates by briefly immersing the glass plates in distilled water. Subsequently, the dry membranes were obtained by drying the *m*-PBI film in between two paper towel covered glass plates at 70 °C *in vacuo* for 3 h.

2.2.2. Membrane pretreatment

The *m*-PBI membrane pieces were soaked in their respective alkaline pretreatments for 24 h before being lightly dried with a paper towel and immediately transferred into 2 M H_2SO_4 to soak for a known time. For cases of no alkaline pretreatment, the dry membrane films were immersed directly in 2 M H_2SO_4 to soak for a known time. The acid step is necessary to protonate, or dope, the polymer as earlier described and to essentially equilibrate the material in an acid analogous to the battery electrolyte to be used.

2.2.3. Uptake measurements

Rectangular 40 x 20 mm samples were punched from the *m*-PBI film and dried in a vacuum oven at 60 °C and 100 mbar overnight before the initial dry weights (wt_{dry}) of the samples were measured. The samples were then soaked in their respective alkaline pretreatment solutions or 2 M H_2SO_4 (in approximately 30 mL of solution in individual vials) for 24 h. For membranes that had undergone both alkaline pretreatment and immersion in acid, these samples were then transferred directly into 2 M H_2SO_4 for an additional 24 h before measuring. The wet samples were lightly dried with a paper towel to remove only the liquid from the membrane surface before their wet weights (wt_{wet}) were measured. The swollen films were then dried in a vacuum oven at 60 °C and 100 mbar overnight before their final dry weights ($wt_{dry\text{-}f}$) were measured. Using the following equations the different uptake and dimensional stability characteristics could then be determined:

$$Uptake_{total}\ (\%) = \frac{wt_{wet} - wt_{dry}}{wt_{dry}} \times 100 \quad (1)$$

$$Uptake_{acid/base}\ (\%) = \frac{wt_{dry-f} - wt_{dry}}{wt_{dry}} \times 100 \quad (2)$$

$$Uptake_{water}\ (\%) = (uptake_{total} - uptake_{acid/base}) \times 100 \quad (3)$$

At least three membrane samples were used for each pretreatment studied, from which mean averages and standard deviations for each uptake characteristic were calculated.

2.2.4. Swelling measurements

The swelling properties of *m*-PBI in the various pretreatments were determined through the analysis of three square (24 x 24 mm) membrane samples. These samples were dried *in vacuo* overnight at 70 °C, after which their dry width (w_{dry}), length (l_{dry}) and thickness (t_{dry}) were measured using a caliper and a thickness gauge (Heidenhain, Messstativ MS200, 224154–01). The dry samples were then immersed in their respective alkaline solution for 24 h before measuring their base swollen dimensions. Followingly, the membranes were immersed in 2 M H_2SO_4 for an additional 24 h, after which their acidic swollen dimensions were measured. The thickness, in-plane and volume swelling of the membranes was determined using eqs. (4)–(6), with t_{wet}, l_{wet} and w_{wet} being the corresponding wet thickness, length and width after equilibrating in the alkaline or 2 M H_2SO_4 solutions, with the provided error being the standard deviation over the three swelling measurements.

$$Thickness\ swelling\ (\%) = \frac{t_{wet} - t_{dry}}{t_{dry}} \times 100 \quad (4)$$

$$In-plane\ swelling\ (\%) = \frac{l_{wet} - l_{dry}}{l_{dry}} \times 100 \quad (5)$$

$$Volume\ swelling\ (\%) = \frac{(l_{wet} \times w_{wet} \times t_{wet}) - (l_{dry} \times w_{dry} \times t_{dry})}{(l_{dry} \times w_{dry} \times t_{dry})} \times 100 \quad (6)$$

2.2.5. Determination of the water and electrolyte volume fraction

The water and corresponding electrolyte volume fraction within the swollen *m*-PBI membranes was determined through the analysis of their water content using Karl-Fischer titration (C30S coulometric KF titrator with InMotion KF oven, Mettler Toledo). Three samples (22 x 22 mm) were prepared from a larger *m*-PBI membrane film with a thickness of ~18.5 μm that was dried *in vacuo* at 80 °C for 5 h. Subsequently, the dry weight of each sample was measured before immersing the samples into their respective alkaline pretreatment solution for 24 h. The samples were then equilibrated in 2 M H_2SO_4, with the width, length and thickness of the samples being measured after 24 h. The acid swollen membranes were immersed in deionized water for 72 h, with the water being refreshed multiple times over this duration until a stable pH between 4 and 5 was reached. Subsequently, the width, length and thickness of the water swollen sample was recorded, from which their volume was calculated. Then, the droplets on the surface of the water swollen film were removed and its weight was measured inside an enclosed vial with a known weight. The water content in the sample was then measured using the mentioned Karl-Fischer titration setup. Here, the water inside the film was evaporated at 180 °C, with the water vapour being titrated. The volume fraction of the water within the membrane (φ_w) was calculated according to eq. (7), with m_{water} being the mass of the titrated water, ρ_{water} the density of water and $v_{membrane}$ the volume of the swollen membrane.

$$\Phi_w(\%) = \frac{m_{water}}{\rho_{water} \times V_{membrane}} \times 100 \quad (7)$$

2.2.6. Through-plane ionic conductivity

Through-plane ionic conductivity measurements were conducted using an SP-300 Biologic potentiostat and EC–LAB software (v11.43). The cell set-up consisted of two platinum disk electrodes (15 mm diameter) with welded-on stainless steel rods. Typically, six 18 mm diameter samples were punched out of membranes in their wet state in 2 M H_2SO_4. The wet samples were sandwiched between the platinum disks before the disks were clamped together using two clips. To prevent conductive contact with clamping clips, acrylic "skirt" pieces slid over the rods were used to cover the underside of the platinum disks. Connecting cables were clipped to the ends of the steel rods and galvanostatic impedance measurements were taken. A sequence of 1-2-3-4-5 membranes were measured, stacking the samples carefully to ensure the absence of air bubbles between the samples, and testing varying combinations of the six samples to take at least two measurements for each number of membranes. Galvanostatic impedance measurements were conducted in the frequency range 150 kHz-25 kHz, with 50 to 100 points taken per decade. The high frequency intercept was extracted for each measurement and plotted against the number of stacked membranes. A linear fit was applied to the data points to obtain the slope, which represents the incremental increase in resistance with stacking, and, subsequently, an estimate for the resistance of a single membrane sample. The area-specific resistance (ASR) of the membrane was then calculated using this resistance value and the active area of the electrode in cm^2 as follows:

$$ASR\ \left(\Omega \cdot cm^2\right) = slope \times A_{electrode} \quad (8)$$

The mean average thickness of the six wet membrane samples (t) in cm and the determined ASR were then used to obtain a value for through-plane ionic conductivity (σ) as follows:

$$Ionic\ conductivity,\ \sigma\ \left(S \cdot cm^{-1}\right) = \frac{t}{ASR} \quad (9)$$

2.2.7. Mechanical strength

1 x 10 cm samples were punched out from the membranes in their 2 M H_2SO_4 wet state. The samples were lightly dried with a paper towel to remove only the liquid from the membrane surface before their swollen thicknesses was measured. Subsequently, they were placed in a tensile testing machine (ZwickRoell Z005, T1-FR005TE.A50). The samples were analyzed at a drawing speed of 500 $mm \cdot min^{-1}$. Mean averages for the tensile strength and Young's modulus values were determined from at least three sample measurements. For stability tests, measurements were taken after the membranes spent 24 h and/or 3 days immersed in 2 M H_2SO_4, and then after 1, 2 and 4 weeks in total. It should be noted that a different piece of cast film was used for each measurement due to the limited size of an individual cast film piece. Therefore, some degree of error between measurements could be expected due to sample variation.

2.2.8. Vanadium (IV) permeability

The diffusion of VO^{2+} through the membranes was measured using custom-made cells with a 10.1 cm^2 active area (diameter 3.6 cm, Fig. S1). The swollen thicknesses of the wet pretreated membranes were measured before they were placed between two ring-shaped ice-cube seal frames. The membrane and seals were sandwiched between the two glass halves of the cell using a clamp. 75 mL of 1.6 M $VOSO_4 \cdot xH_2O$ (≥97 %, Sigma Aldrich, the hydration content of which was determined by UV–Vis absorbance using a calibration curve made with a vanadium standard, Fig. S2) in 2 M H_2SO_4 was placed into one tank of the cell and 75 mL of 1.6 M $MgSO_4$ (≥99.5 %, anhydrous, Reagent Plus®, Sigma-Aldrich) in 2 M H_2SO_4 was placed into the other. A magnetic stirrer bar was placed into each tank before they were sealed lightly with rubber bungs. The solutions were stirred at room temperature throughout the experiment. 2.5 mL aliquots were taken from the $MgSO_4$ side approximately every 24 h and placed in a quartz cuvette (10 mm path length, Hellma analytics) for UV–Vis absorbance measurements (Agilent Cary 4000 spectrophotometer). If not diluted, the aliquot was returned to the original tank after analysis in order to avoid significant changes in volume over the experiment. Dilutions were made when the absorbance at 765 nm was above 1 by adding 2 M H_2SO_4 to a 0.25 or 0.5 mL aliquot to prepare a 2.5 mL sample (10x or 5x dilution). The VO^{2+} absorbance peak at 765 nm was used to calculate the VO^{2+} concentration in the vanadium-deprived half of the cell (C_D) using a calibration curve (Fig. S2). The diffusion coefficient of

VO^{2+} (D_{VOSO4}) was calculated according to the equation:

$$D_{VO^{2+}}\left(cm^2{\cdot}\min^{-1}\right) = \frac{d(C_D(t))/dt \times V_D}{A \times (C_E - C_D(t))} \times t \quad (10)$$

where $d(C_D(t))/dt$ is the concentration versus time slope in $mol{\cdot}L^{-1}{\cdot}min^{-1}$, V_D is the solution volume of the $MgSO_4$ side in mL, A is the active area of the membrane in cm^2, t is the wet thickness of the membrane in cm, C_E is the concentration of $VOSO_4$ in the enriched side of the cell, C_D is the concentration of $VOSO_4$ in the deprived part of the cell ($MgSO_4$ side).

2.2.9. VRFB cell set-up

Cell operations were performed using a laboratory-scale cell with an active area of 25 cm^2 (5 x 5 cm) and an electrochemical test station (Scribner Model 857 test stand, Scribner Associates, Southern Pines, NC, USA). The test stand was equipped with two in-house designed 70 mL glass tanks and two peristaltic pumps (Masterflex L/S®, GZ-07522–20, Cole Parmer GmbH, Wertheim, Germany), all attached using plasticizer-free chemical resistant tubing (Versilon™ 2001, GZ-06475–16, Cole-Parmer GmbH, Wertheim, Germany). Data was collected using Flow-cell™ software and processed and analyzed using BView (Scribner Associates).

The electrochemical cell was assembled by sandwiching between the two end plates of the cell: two gold-plated copper current collectors (Scribner Associates), two triple-serpentine graphite flow fields (Scribner Associates), two in-house designed gaskets consisting of polyvinylidene fluoride (PVDF) frames (7.6 x 7.6 cm, 2.5 mm thickness) with ice-cube seals, two 5 x 5 cm carbon felt electrodes (Type AAF304ZS, Toyobo, Osaka, Japan) and the pretreated wet membrane sample. The cell was tightened with frame bolts gradually to 4 N·m using a ratchet, resulting in a felt compression of approximately 42 %.

2.2.10. VRFB cell cycling procedures

For all cycling experiments, 40 mL of electrolyte (1.694 M V) was placed into each glass tank and was purged with argon at 66 $mL{\cdot}min^{-1}$ throughout the experiment. An electrolyte flow of approximately 60 $mL{\cdot}min^{-1}$ was used for the experiments by controlling the pump speed. Before cycling, the membrane and carbon felt electrodes were allowed to condition under electrolyte flow (average vanadium oxidation 3.5, −50 % state of charge (SoC)) at open circuit conditions for 4 h. Impedance measurements were taken at open circuit voltage after the 4 h of conditioning to measure the *in situ* through-plane ohmic resistance of the cell at −50 % SoC, measured between 10 kHz and 0.1 kHz with a perturbation amplitude of 100 mV. The cell resistance was determined from the y-intercept of a slope obtained by plotting the *in situ* ohmic resistances of 1 through 6 stacked Nafion™ NR212 membranes measured in cell tests after 4 h at open circuit conditioning under electrolyte flow (−50 % SoC). The cell resistance (242 $m\Omega{\cdot}cm^2$) was then subtracted from the *in situ* ohmic resistance of each cell tests to determine the area-specific resistance (ASR) of the membrane. For the screening cycling tests, the cell was charged to 100 % SoC in a step-wise manner at a current density of 80 $mA{\cdot}cm^{-2}$. Polarization curves were recorded at 30, 50 and 70 % SoC during this charging process by consecutively charging and discharging for 20 s at current densities of 20, 40, 60, 80, 100, 120, 150 and 200 $mA{\cdot}cm^{-2}$. Once fully charged, the system was consequetively cycled for: 10 times at a current density of 80, 120, 160, 200 and 240 $mA{\cdot}cm^{-2}$, 5 times again at 120 $mA{\cdot}cm^{-2}$, 20 times at 240 $mA{\cdot}cm^{-2}$, and a final 5 times at 120 $mA{\cdot}cm^{-2}$. For the additional cycling tests, the system was cycled for 10 times at 80, 20 times at 120, and then 10 times each at 160, 200 $mA{\cdot}cm^{-2}$ and then 120 $mA{\cdot}cm^{-2}$ once again. The charge/discharge cycles were performed between 0.80 V and 1.65 V as the respective lower and upper potential limits. The first cycle at each current density was not included in the analysis due to the influence of the prior current density. Efficiencies and discharge capacity were calculated according to the following equations:

$$Coulombic\ efficiency,\ CE\ (\%) = \frac{Q_{dis}}{Q_{ch}} \times 100 \quad (11)$$

$$Voltaic\ efficiency,\ VE(\%) = \frac{\bar{U}_{dis}}{\bar{U}_{ch}} \times 100 \quad (12)$$

$$Energy\ effficiency,\ EE\ (\%) = CE \times VE \quad (13)$$

$$Theoretical\ maximum\ capacity,\ Q_{theoretical} = n \times F \quad (14)$$

$$Discharge\ capacity,\ DC\ (\%) = \frac{Q_{dis}}{Q_{theoretical}} \times 100 \quad (15)$$

Where: Q_{dis} and Q_{ch} are the capacities of the discharge and charge process, respectively; $\bar{U}_{dis}$ and $\bar{U}_{ch}$ are the average discharge and charge potentials, respectively; n is the total number of moles of active redox species and F is the Faraday constant ($96{,}485 C{\cdot}mol^{-1}$).

For extended cycling tests, following open circuit conditioning for 4 h the cell was charged to 100 % SoC at a current density of 120 $mA{\cdot}cm^{-2}$. The cell was then cycled at 120 $mA{\cdot}cm^{-2}$ for 100 cycles (approximately 100 h).

Capacity fade, $mAh{\cdot}h^{-1}$, was determined by applying a linear fit over the discharge capacities (mAh) of the first 20 cycles at 120 $mA{\cdot}cm^{-2}$ plotted versus the experimental time (h) to obtain a slope. The first cycle was always omitted in analysis due to the deviation caused by the jump in current density from the previous cycle. For the extended cycling tests, the capacity fade in $mAh{\cdot}h^{-1}$ was determined by applying a linear fit to the discharge capacities (mAh) over the whole test plotted versus the cycling duration (h) to obtain the slope. Similarly, the first cycle was omitted from analysis.

3. Results and discussion

3.1. Dimensional swelling and uptake of base and acid

The effects of an alkaline pretreatment on the dimensional swelling of *m*-PBI were examined by subjecting membrane samples to immersion in various hydroxide solutions and concentrations, from LiOH to CsOH. The hydroxide solutions used were chosen to study the influence of an increasing size of the alkali cation and their concentration on the properties of the swollen membrane. Dry weight and dimension measurements were taken of samples punched from cast *m*-PBI films and were then remeasured either after soaking in their respective alkaline pretreatment for 24 h (denoted: e.g. 4Na = membrane pretreated in 4 M NaOH for 24 h) or after acid treatment for an additional 24 h directly succeeded (denoted: e.g. 2Na2K2S = membrane pretreated in 2 M NaOH-2 M KOH for 24 h, followed by 2 M H_2SO_4 for 24 h). Levels of water and acid/base uptake were also calculated after drying the swollen samples once again before weighing.

All alkaline pretreatments resulted in thickness swelling of the *m*-PBI material, up to a maximum of 120 % observed for 2Cs (Fig. 1A). Interestingly, in-plane shrinking was observed for larger cations and higher base concentrations suggesting that swelling is anisotropic in nature, which has been observed for both acid and base–doped PBI membranes [25,31]. This is thought to be due to the removal of the lamellar regions of PBI upon contact with a strong acid or base and the corresponding rearrangement of the polymer chains [32,33]. Thickness and volume swelling was found to generally increase with ascending alkali cation size as well as with molarity, from 2 to 4 M. On deprotonation of the benzimidazole groups in *m*-PBI and association with alkali cations, it can be expected that larger alkali cations cause more disruption to interactions between PBI chains, resulting in greater space expansion and enabling a higher base and water uptake. The general increase observed in both base and water uptake with alkali cation size and solution concentration also supports this.

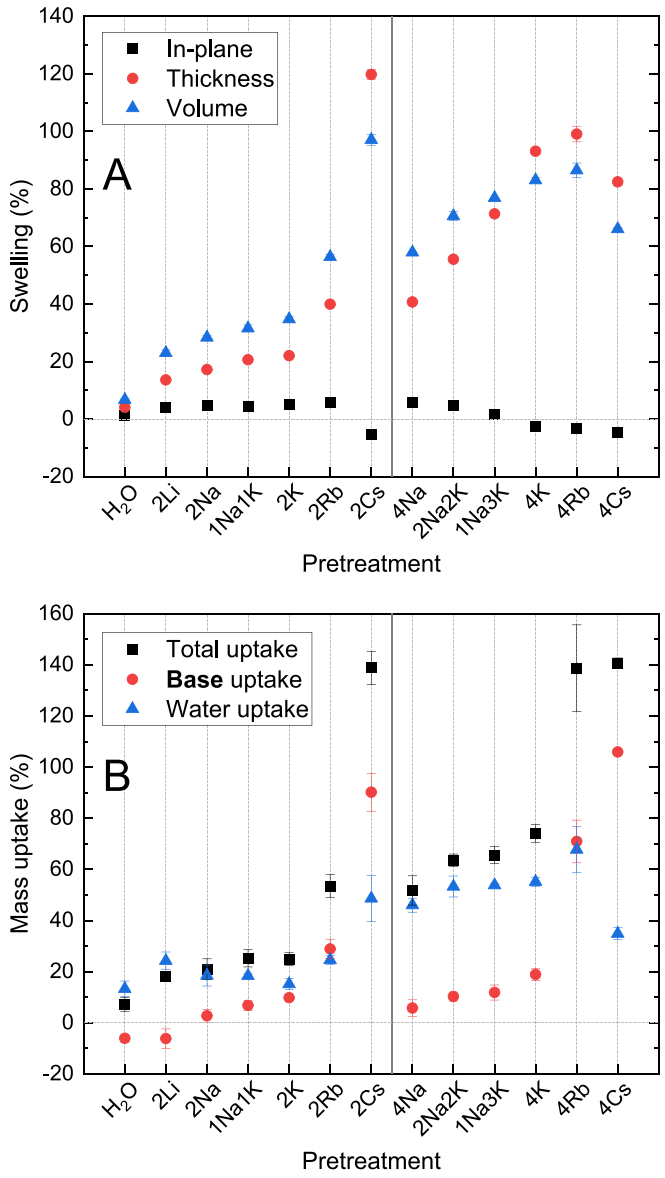

Fig. 1. A) Thickness, in-plane and volume swelling and B) mass uptake characteristics of various alkaline hydroxide pretreatments conducted on m-PBI, with the given error being the standard deviation over the measurements. Notation: e.g. 2Na2K = m-PBI immersed in 2 M NaOH-2 M KOH for 24 h.

Notably, the two NaOH and KOH mixtures, 1Na3K and 2Na2K, resulted in swelling levels that were intermediate to those of the 4 M treatment counterparts, 4Na and 4 K. In addition, 2Na2K > 2 K swelling, indicating that mixtures of alkali cations can impart cumulative swelling effects. However, a deviation from the general swelling trend was observed for 4Cs, with unexpectedly low swelling despite its high base uptake. For this sample, visible material damage (crinkling and increased brittleness) was observed, indicating an excessively aggressive pretreatment which may have caused highly irregular morphology changes and structure collapse. It should also be noted that the hydroxide treatment solutions for 2Cs, 4Rb and 4Cs developed a yellow color after 24 h, with 4Cs being the darkest, a further indication that membrane damage can occur at these conditions. Similar observations were reported for concentrated acidic solutions used to immerse PBI, proposed to be due to the dissolution of low molecular weight polymer fractions from amorphous PBI regions [25]. Reductions in the overall weight of PBI membranes treated in KOH solutions have also been attributed to the loss of smaller polymer fractions, shown to be enhanced after extensive exposure at high hydroxide concentrations and elevated temperatures and to be a result of base hydrolysis and subsequent scission of PBI chains by ring-opening [30,34–36]. Considering this, the observations in this work are proposed to be due to a combination of the dissolution and alkaline hydrolysis of low weight polymer fractions that was more extensive in the Cs and Rb soaked membranes because of the highly amorphous structures they possess as a result of more forceful swelling.

In the cases which included an additional acid treatment step, the films shrunk slightly in their thickness and in–plane dimensions relative to post-alkaline treatment, but importantly, were not reduced to the 2S sample values (Fig. S3A). This indicated that the alkaline treatments maintained a substantial degree of their effect on the *m*-PBI morphology in the protonated polymer form. The acid uptake for all membranes exceeded that of their base uptake, except for 2Cs, 4Rb and 4Cs, here, the variation in water uptake was more random. (Fig. S3B). Although these observations are difficult to explain, it is important to regard the complexity of the membrane system, particularly the various mechanisms and driving forces of ion and water transport that are at play, in addition to the microstructure of the polymer. For example, the trend of water uptake and swelling in Nafion™ membranes has been observed to be the opposite to that in this work, actually decreasing with the size of alkali cation, and was theorized to be due to an elaborate combination of factors including cation mobility and hydration shells, to name a few [45,46].

3.2. Water and electrolyte volume fraction

In the previous section, the dimensional swelling and electrolyte uptake of an *m*-PBI membrane was shown to generally increase with increasing hydroxide concentration and alkali cation size. To understand this phenomenon, the water volume fraction of the membrane was determined as described in section 2.2.5. In each pretreatment step, the volume of the polymer electrolyte changes due to its affinity to the electrolyte solution and its prior morphology. Despite this, the volume occupied by the polymer itself does not change, with the change related to the electrolyte volume fraction within the film. However, measuring the electrolyte volume fraction in either the alkaline or acidic treatment step is difficult as the electrolyte concentration inside the film is vastly different to that of the bulk solution. Consequently, the membranes were washed multiple times in deionized water after completing all pretreatment steps to fully exchange the acidic electrolyte with deionized water. The effectiveness of this exchange was confirmed by drying test membrane samples, leading to their weight prior to the pretreatments being recovered. Now, instead of a complex polymer electrolyte system, a system is obtained where the polymer electrolyte only consists of the polymer itself and water. Although the density of imbibed water inside a polymer film can differ slightly from the bulk solution as shown by Wu et al. [37], a significant change from 0.997 g·mL^{-1}, the density of water at 25 °C, is not expected to occur. Considering this, the water content and with that the water volume fraction of the swollen membrane can be measured with a Karl-Fischer titration. Using this water volume fraction and the volume shrinkage upon exchanging the acidic electrolyte with deionized water (~8–10 %, Table S1), the volume fraction of the electrolyte within the membrane after pretreatment can be determined, Fig. 2. The water volume fraction is shown to increase with increasing cation size, closely following the trends previously observed. The lowest value is obtained for *m*-PBI swollen in water, respectively 24 ± 1 v.%, whereas the 2Cs2S pretreatment leads to an increase of water content to 47 ± 1 v.%. In the acidic pretreatment step, the same trend is seen, with the lowest electrolyte volume fraction obtained for a membrane only swollen in 2 M H_2SO_4 at 35 ± 1 v.%. On the contrary, this volume fraction increases to 40 ± 3 v.%, 44 ± 1 v.% and 52 ± 1 v.% for respectively the 4Na2S, 4K2S and 2Cs2S pretreatments. These results show that in addition to the increased dimensional swelling and electrolyte uptake, the electrolyte volume fraction also increases as a result

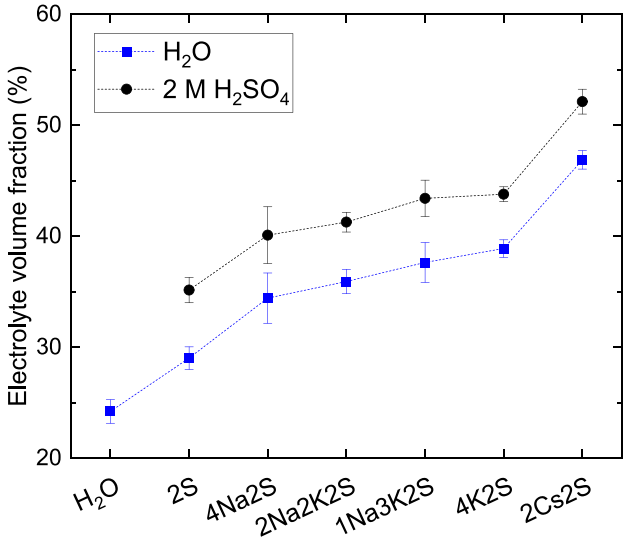

Fig. 2. The electrolyte volume fraction within an m-PBI membrane after various pretreatments in the H_2O exchanged and the corresponding pretreatment form in 2 M H_2SO_4. A dashed line between the data points is added as a guide to the eye.

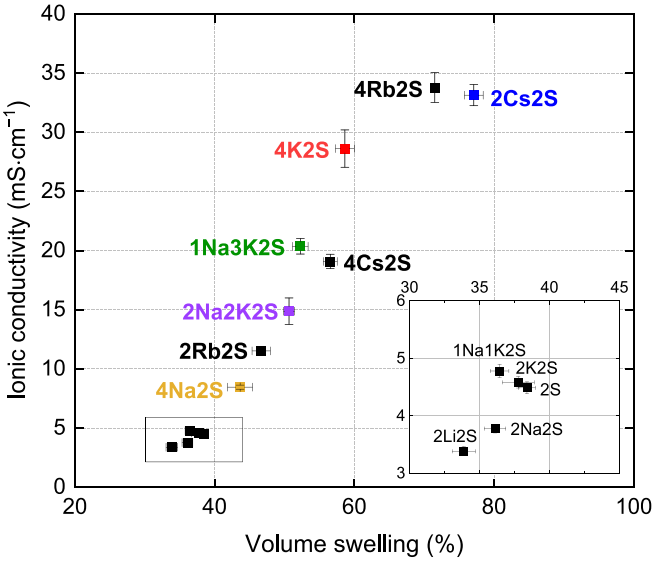

Fig. 3. Plot of the ionic conductivity vs. volume swelling of the pretreated m-PBI membranes, measured in 2 M H_2SO_4. Inset shows a zoom of the area indicated in the box.

of the alkaline treatment, thereby proving its effectiveness. Although this effect can be beneficial for the ionic conductivity of the polymer electrolyte, the increased electrolyte volume fraction can also have adverse effects for its vanadium barrier properties due to the more open polymer electrolyte structure, thereby indicating the importance of a detailed membrane characterization.

3.3. Conductivity

The relationship between the volume swelling and the ionic conductivity of the membrane in 2 M H_2SO_4 was then studied. Significant increases in conductivity from that of the untreated membrane, 2S, (4.5 mS·cm^{-1}) appeared to only occur once total alkaline concentrations higher than 2 M were used or the alkali cation was Rb^+ or larger (Table S2). This was in line with the volume swelling and uptake characteristics, seeing as the acid and water uptake as well as volume swelling of the membranes 2Li2S through to 2K2S were comparable or lower than 2S (Fig. S3). In acid-doped PBI, conductivity is attributed to a number of charge carriers and mechanisms, including the transfer, or 'hopping', of protons between the N/N-H sites of the benzimidazoles and the ions and water in the acidic electrolyte via the formation and breaking of hydrogen bonds, and conduction via the charge carrier ions of the dissociated 'free' acid in the membrane [16,38,39]. Conductivity is influenced by a complex combination of factors, including the acid and water uptake by the polymer, the polymer morphology and the effective concentration of the absorbed solution. Generally, a positive trend between conductivity and volume swelling was observed (Fig. 3), as a greater electrolyte volume fraction and, therefore, more open polymer packing structure was observed for higher swelling degrees, allowing for higher acid and water uptake.

In correlation with the swelling and uptake data, a maximum was reached for 4Rb and 2Cs at ~34 mS·cm^{-1} and not for the overly damaged 4Cs membrane which exhibited a decreased conductivity due to its lower swelling. With focus on the Na-/K-OH treated membranes, an increase in conductivity from 2S by ~2 times was seen for 4Na2S in contrast to ~6 times for 4K2S, whilst those for 2Na2K2S and 1Na3K2S could be seen to sit almost proportionately in-between.

To monitor the stability of the material properties over time, through-plane ionic conductivity measurements were additionally taken periodically over 15 weeks of storage in 2 M H_2SO_4. In general, the conductivities of each membrane remained relatively constant over the period of study, along with their measured thicknesses, suggesting that they do not return to their untreated state and can retain their associated characteristics, regarding composition and morphology, over a long time frame (Fig. S4). Minor fluctuations (ranging by 4–5 mS·cm^{-1}) were observed more frequently for the more swollen membranes, 2Na2K2S, 1Na3K2S and 4K2S, although error bars in these measurements were also larger. This was likely due to their higher susceptibility to experience effects of thickness compression on their pressing between the electrodes during the experimental set-up and during the thickness measurement.

3.4. Vanadium (VO^{2+}) permeability

As the crossover of vanadium ions primarily leads to reductions in coulombic efficiency (CE) and increasing rates of capacity fade/self-discharge, minimizing vanadium permeability through a membrane is of key importance, but must be achieved through a fine balance of material characteristics and/or with careful polymer design. The permeability of the pretreated *m*-PBI membranes to vanadium ions (VO^{2+}) was studied using a custom-made diffusion cell set-up, measuring the increasing concentration of VO^{2+} in an initially V-deficient compartment over time through UV–Vis absorption spectroscopy (see section 2.2.8). The 2S and 2Cs2S membrane samples were tested to represent the two extremities of volume swelling and the four membranes pretreated with NaOH and/or KOH solutions were selected for study as being in the intermediate range of interest. The 4Rb2S and 4Cs2S samples were not analyzed due to their increased brittleness in combination with the observed discoloration of the alkaline solution. Notably, the most swollen membrane, 2Cs2S, exhibited a vanadium diffusivity that was slightly higher than that of Nafion™ NR212 (NR212), because of its overly open structure (Fig. 2). On the other hand, all four of the other pretreated membranes studied were a significant improvement on NR212, implying they retain sufficient electrostatic repulsion (Donnan exclusion) of vanadium at their levels of swelling (Fig. 4, Table S3). The upward trend in permeability across the four Na-/K-OH treated membranes was in agreement with their order of volume swelling. Furthermore, a decrease in selectivity, a parameter calculated using the *in situ* area specific resistances (ASR) of the membranes and a measure of vanadium permeance expressed as a current density (see equations S1, S2) [40,41], also followed this trend, consequential of a more expanded polymer chain packing structure (Fig. S6,

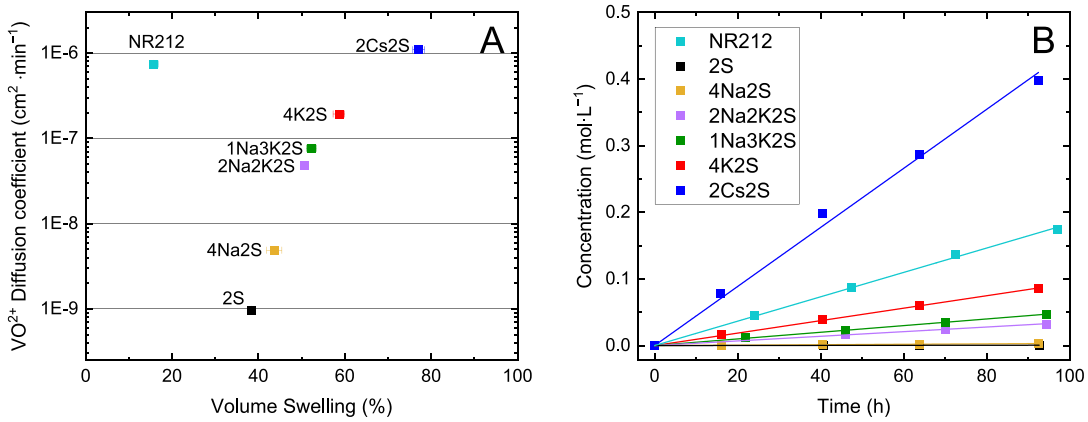

Fig. 4. A) comparison of the VO^{2+} diffusion coefficients determined for the pretreated membranes plotted against volume swelling, and B) Concentration vs. time slopes plotted for various pretreated membranes using the change in intensity of the VO^{2+} absorbance peak at 765 nm.

Table S3). Permeance to vanadium displayed by 4Na2S was approximately 6 times worse than 2S, whereas it was approximately 60 times worse for 2Na2K2S, attributed to their increased swelling (Fig. 1A, Table S3). On the other hand, relatively subtler differences in permeance and selectivity were seen between 2Na2K2S, 1Na3K2S and 4K2S, which prompted interest in a close comparison of their performance in VRFB cell cycling tests.

3.5. Mechanical strength

The pre-swelling of PBI with alkaline or acid treatments generally results in decreased mechanical strength due to the reduced intermolecular interactions between polymer chains [26,35]. The four Na-/K-OH pretreated membranes along with 2S were selected for mechanical strength testing, and measurements were taken after varying times spent stored in 2 M H_2SO_4 to monitor stability. All membranes appeared to be stable regarding their mechanical characteristics over the testing period of four weeks (Fig. S7–10). In comparison to 2S, the tensile strength and Young's modulus of all the pretreated membranes were expectedly lower and in order of their degree of volume swelling. Notably, 2Na2K2S, 1Na3K2S and 4K2S had only little variation between them, displaying 35, 30 and 25 MPa in tensile strength, respectively.

3.6. Thicker membranes

The effect of the *m*-PBI film thickness on the pretreatment methodology was briefly investigated, seeing as thicker membranes are generally less prone to breakage during handling or to pinhole formation during cell tests from carbon fibre punctures or effects of compression. Thicker variants of the *m*-PBI films were also prepared as described in the Experimental Methods, section 2.2.1, with a dry thickness of 35 μm, pretreated in the same fashion and tested for their mechanical strength and conductivity. Only the four Na-/K-OH pretreatments of focus were applied to the thicker membranes for a brief comparison. For the thinner and thicker membranes in each couple, their ionic conductivity was comparable (Fig. S4), due to proportionate increases in both swollen thickness and ohmic resistance, and mechanical stability differed insignificantly (Fig. S9–10). As the same trends in characteristics (increasing conductivity and decreasing mechanical strength) were also observed for both variants, the effects of the alkaline pretreatments and acid doping on the *m*-PBI morphology could be assumed to be analogous in both material thicknesses. This indicates a level of flexibility in the adoption of this alkaline pretreatment methodology, in that the thickness of the PBI membrane could also be selected or fine–tuned depending on the operator's resources and the membrane's application. However, as the *in situ* ohmic resistance will increase with *m*-PBI thickness, which can be expected to result in decreased energy efficiencies (EEs) in a VRFB cell [42], the thinner variants of the pretreated membranes were put forward for cell testing in this study.

3.7. Cell cycling performance

3.7.1. Single cell tests

The membranes analyzed in the diffusion cell experiments were selected for screening tests in a VFRB single cell, including the membranes at the two ends of the spectrum in terms of degree of volume swelling, 2S and 2Cs2S (Fig. S11). The particularly promising four Na-/K-OH pretreated membranes were then put forward for further cycling tests for closer investigation. All the pretreatments appeared to have improved performance to that of 2S in terms of EE, with the trends in EEs and voltaic efficiencies (VE) generally following that of the membrane conductivities (Fig. S11). This showcases that although the selectivity is an important membrane property, it is only one part of the story. Whereas, the selectivity was shown to decrease for all pretreatments compared to 2S, the EE, which is generally governed by the selectivity, actually increases. This behaviour can be explained by the extremely low vanadium permeability of *m*-PBI. This low permeability gives all *m*-PBI membranes a coulombic efficiency close to a 100 %, with a small decrease seen upon increasing the membrane swelling, as a result of the increased electrolyte volume fraction within the membrane and corresponding vanadium diffusivity. Despite this increase in diffusivity through the membrane, even almost 200 times higher for 4K2S compared to 2S, the value by itself remains fairly small. Furthermore, in a VRFB cell, the vanadium crossover is not only governed by the diffusivity, as vanadium migration, originating from the applied current density, plays a significant role [43]. As such, in this case, the improvement in ionic conductivity (~6 times higher for 4K2S compared to 2S) is actually more beneficial for the system than the adverse effects of the decreased selectivity.

The cell assembled using the most swollen membrane, 2Cs2S, exhibited the highest VEs throughout the test due to it having the highest ionic conductivity and lowest *in situ* ASR (Table S4). However, it suffered from vast capacity fade that was markedly comparable to that of NR212 due to its similarly high vanadium diffusivity, (Fig. S11D, Table S3), which was also reflected in its lower CEs in comparison to other *m*-PBI membranes. Due to its still high ASR (Table S4), the performance of the least swollen pretreated membrane tested, 4Na2S, was not a significant improvement on 2S, with EEs only moderately higher throughout. On the other hand, 4K2S, 1Na3K2S and 2Na2K2S all offered substantially higher EEs, with the difference in their VE compared to that of 2S at a given current density being correlated to their ASRs (Table S4). Furthermore, the demonstrated discharge capacities range from ~54 % to ~65 % when cycling at 240 $mA{\cdot}cm^{-2}$ in contrast to only ~41 % and ~18 % exhibited by 4Na2S and 2S, respectively. In addition,

they showed excellent recovery in EE, returning to a ~85 % energy efficiency at 120 mA·cm^{-2} after cycling at a high current density of 240 mA·cm^{-2}.

As the effects of the different Na-/K-OH pretreatments on capacity fade were still unclear at this stage, additional cell tests including more cycles (20x) at 120 mA·cm^{-2} were conducted. 4K2S, 1Na3K2S and 2Na2K2S again resulted in comparable cell performance, all achieving excellent average EEs of ~85 % at 120 mA·cm^{-2} and exhibiting high and stable discharge capacities of 91–93 % over this period of 20 cycles (Fig. 5). Capacity fade (given as the slope of the discharge capacities of each cycle plotted versus time, see section 2.2.10) during the cycles at this current density was markedly similar between the membranes, but a subtle trend could be identified: 4K2S (-1.7 ± 0.2 mAh·h^{-1}) > 2Na2K2S (-0.9 ± 0.1 mAh·h^{-1} > 1Na3K2S (-0.05 ± 0.08 mAh·h^{-1}). In addition, a subtle trend could be seen for the capacity utilization, with 4K2S showing the highest discharge capacity, which can be attributed to its lower ASR (Table S4).

It should be noted that variations in measured ASRs as well as efficiencies were observed during cell test repeats for each membrane, which could largely be due to small inconsistencies in compression and membrane thickness between cell tests. The swollen morphologies of the membranes will be somewhat prone to compressive forces on cell assembly, resulting in a thinner, denser membrane. Thereby, the ohmic resistance of the active membranes will differ slightly between cell tests and give rise to discrepancies which can be expected to worsen with degree of thickness swelling. The particularly fine differences in cell performance between 4K2S, 1Na3K2S and 2Na2K2S may in part be due to these effects, seeing as they possess comparable swollen thicknesses and material properties. The similarity in the ohmic resistances of the membranes is also expressed in the measured polarization curves (Fig. S12–13). At all current densities as well as at various states of charges, the slopes of the polarization curves of each membrane were distinctly similar. Plotting the average cycling performances and extrapolating the energy efficiency to higher current density, Fig. S14, a small but noticeable improvement in energy efficiency can be observed for 4K2S pretreated membranes, which is more pronounced at higher current densities. This improvement can be attributed to its slightly lower ASR of 298 ± 28 mΩ·cm^2, versus 333 ± 31 mΩ·cm^2 and 344 ± 27 mΩ·cm^2 for respectively 1Na3K2S and 2Na2K2S, thereby reducing the ohmic losses of the VRFB. In contrast, the energy efficiency of the blended 2Na2K2S and 1Na3K2S pretreatments remains comparable over the entire current density range. Furthermore, the importance of the presence of potassium in the pretreatment solution can be witnessed, with 2Na2K2S, 1Na3K2S and 4K2S all outperforming NR212 over the extrapolated current density range, while 4Na2S and 2S pretreated samples remain worse.

3.7.2. *Extended cycling tests*

The three best performing membranes, 4K2S, 1Na3K2S and 2Na2K2S, were then put forward for extended tests, cycling for 100 cycles at 120 mA·cm^{-2}, over approximately 100 h (Fig. 6). 4K2S displayed the highest rate of capacity fade over the longer time frame, due to its permeability to vanadium and susceptibility to electrolyte crossover, however, it possesses the lowest ASR of the three membranes and displays the highest VE and EE (Fig. 6, Table 1). 1Na3K2S and 2Na2K2S again displayed a similar performance, and retained average energy efficiencies of 84.9 (±0.2)% and 84.2 (±0.4)% over the experimental time frame, respectively. Furthermore, they exhibited comparably high

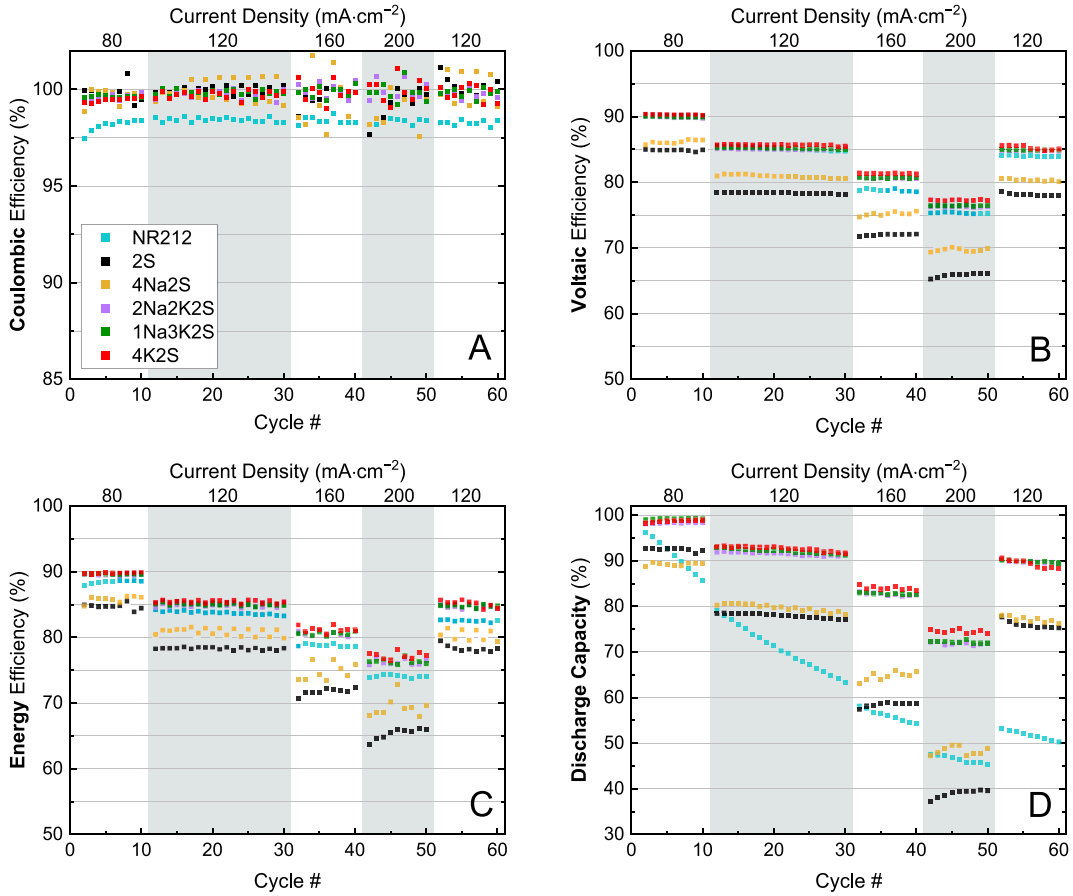

Fig. 5. Short-term cycling test with: A) Coulombic efficiencies, B) voltaic efficiencies, C) energy efficiencies and D) discharge capacities measured using the four Na-/K-OH pretreated membranes and 2S. Cycling for 10 cycles at 80 mA·cm^{-2}, 20 cycles at 120 mA·cm^{-2}, and then 10 cycles each at: 160 mA·cm^{-2}, 200 mA·cm^{-2}, and 120 mA·cm^{-2}.

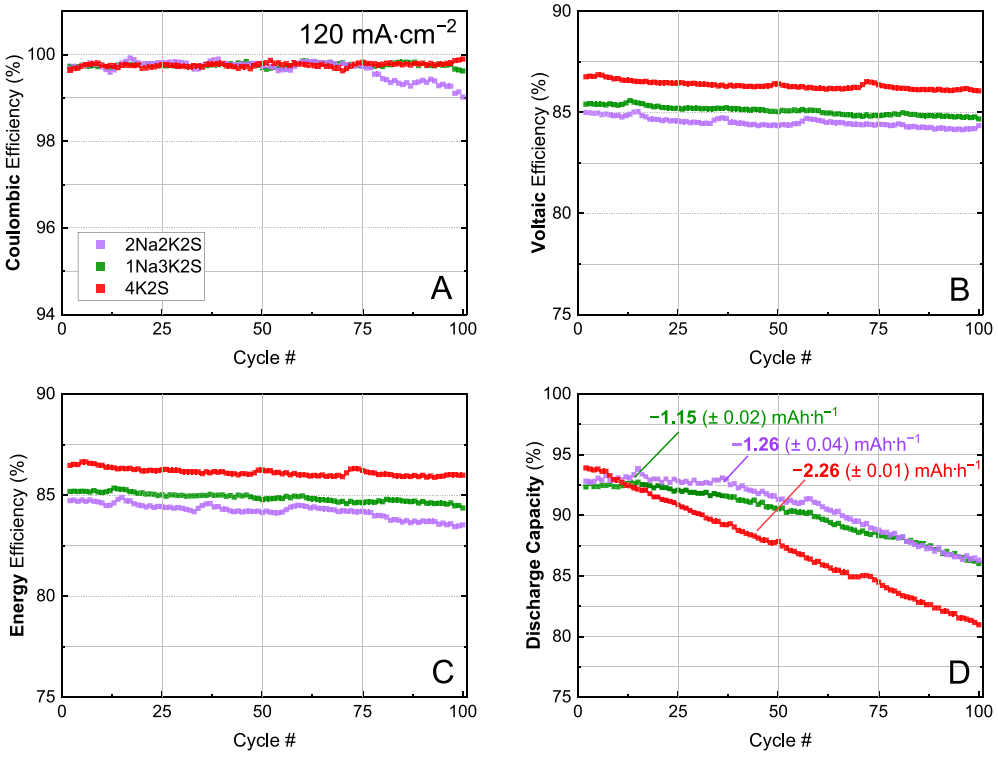

Fig. 6. A) Coulombic efficiencies, B) voltaic efficiencies, C) energy efficiencies and D) discharge capacities measured from extended cell cycling tests using 4K2S, 1Na3K2S and 2Na2K2S, cycling for 100 cycles at 120 mA·cm^{-2} (approximately 100 h). In addition, the discharge capacity fade over 100 cycles is given in D).

Table 1
In situ properties of the three Na-/K-OH pretreated membranes of focus. Capacity fade and electrolyte imbalance are shown for the extended tests cycling at 120 mA·cm^{-2}. DC retention = the% of discharge capacity available at the end of cycling relative to at the start of cycling.

Pretreatment	ASR (mΩ·cm^2)	Capacity Fade over 100 cycles at 120 mA·cm^{-2}		Capacity Fade after 50 h	Electrolyte Imbalance (mL)
		mAh·h^{-1}	DC retention (%)	mAh·h^{-1}	
2Na2K2S	344 ± 27	−1.26 ± 0.04	93.0	−1.86 ± 0.03	3
1Na3K2S	333 ± 31	−1.15 ± 0.02	93.2	−1.47 ± 0.02	5
4K2S	298 ± 28	−2.26 ± 0.01	86.2	−2.30 ± 0.02	6

capacity retention, both holding ~93 % of the discharge capacity they held at the start of cycling after the 100 cycles, and with very similar slow rates of fading (Table 1). Despite the comparable capacity loss, 1Na3K2S experienced a higher electrolyte crossover than 2Na2K2S due to its more open structure. Similarly, the electrolyte imbalance increased further for 4K2S due to its even higher electrolyte volume fraction, Fig. 2. The pattern of the capacity fade of the 2Na2K2S and 1Na3K2S pretreated samples shows a lower capacity fade at the start of the test, before becoming more linear after cycle 40. In contrast, the 4K2S membrane shows the linear capacity fade already after the first few cycles of the test, indicating a faster membrane equilibration, but remaining the highest after 50 h. All membranes show a stable energy efficiency (±1%) over these 100 cycles. Furthermore, as all pretreatments showed a stable through-plane ionic conductivity over 15 weeks and stable mechanical properties over 28 days, a drop in the cell performance due to the membrane stability is not expected. The measured cell performance of the pretreated membranes is among the highest reported in literature as highlighted in the comprehensive review by Xiong et al. [44], with most membranes exhibiting an energy efficiency of 80–85 % at 120 mA·cm^{-2} and a capacity decay rate of 0.14–0.48 % per cycle. The latter corresponds to a loss of capacity of 14–48 % over 100 cycles, showing that alkaline pretreated *m*-PBI membranes can give a lower capacity fade, while maintaining a high energy efficiency.

An operational trade-off presents itself with alkaline pretreatments on *m*-PBI membranes, between the ohmic resistance of the membrane and both its capacity retention capability and its ability to act as a barrier against electrolyte crossover. The ability of the membrane to address this trade-off can be evaluated by plotting the membrane ASR versus the capacity fade measured when cycling at 120 mA·cm^{-2} (Fig. 7). The ideal membrane material would be situated at the top-left corner of the plot, possessing a low area specific resistance and exhibiting minimal capacity fade due to a fine balance of both low resistive losses and low vanadium permeability. In line with experimental results, 1Na3K2S and 2Na2K2S both reside in this ideal region, showcasing that a careful finetuning of the VRFB system is possible, with the mixed Na-/K-OH pretreatments enabling a fine balance of membrane properties. Furthermore, the low cost of a PBI membrane, estimated as less than 10 % of Nafion™ 115 and below 50 USD/m^2 for a 68 μm asymmetric porous PBI membrane by Yuan et al. [14], makes this approach particularly suitable to obtain both membranes with a low ASR and a low capacity fade, with an estimated cost of 10–20 USD/m^2 due the lower thickness (14.5 μm) of our dense PBI membrane. In addition, as the mixed alkaline pretreatments can easily be reused and contain abundant materials, it is not expected that this step adds significant costs to the membrane preparation process.

4. Conclusion

This work provides valuable insight into the swelling behaviour of *m*-PBI in alkaline solutions and the effect on its material properties and consequent performance as an ion-exchange membrane in VRFBs. By

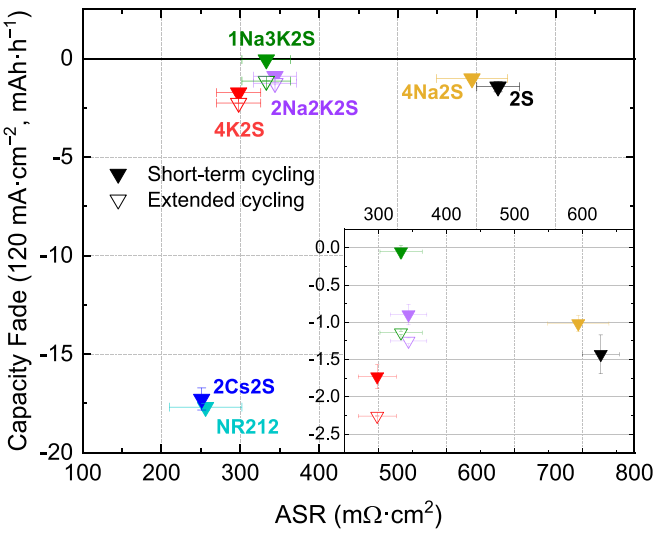

Fig. 7. Figure of merit – *in situ* area specific resistance (ASR) vs. capacity fade of the four Na-/K-OH treated PBI membranes, 2S, 2Cs2S and NR212 during the short-term and extended cycling test. Inset shows a zoom on the region containing 2S and the four Na-/K-OH treated PBI membranes of main focus in the study.

using pretreatment solutions of various alkali hydroxides, as well as mixtures of both KOH and NaOH, lying between 4 M concentrations of each individually, 1 M NaOH–3 M KOH or 2 M NaOH–2 M KOH, optimal membrane characteristics can be achieved through exerting an ideal intermediate level of volume swelling in the PBI. The inclusion of KOH is demonstrated to be necessary for achieving a sufficiently low resistance in the membrane to increase cell capacities otherwise lost to ohmic contributions, and retain high EEs. However, pretreatment in KOH alone (4 M) results in electrolyte crossover that induces capacity fading that becomes significant over extended cycling periods. Increasing the size of the alkali hydroxide further, to RbOH or CsOH, leads to an even greater volume swelling, and with that, an even higher capacity fading as demonstrated by 2 M CsOH treated samples. Consequently, the inclusion of NaOH is proven necessary in order to mitigate the harsher swelling effects of KOH by minimizing capacity fade due to electrolyte crossover effects, but the lower degree of swelling imparted by a solution of NaOH alone (4 M) does not suffice to adequately reduce the ohmic resistance, leading to higher losses in EE. These intermediate swelling levels in PBI result in the best compromise of material characteristics in the membrane, minimal capacity fade and steady, high energy efficiencies of ~85 % when cycling at 120 mA·cm^{-2} over extended periods (~100 h). The tunability of the blended pretreatment approach in this work, as well as its high accessibility due to the low costs of NaOH and KOH, offers the operator additional and valuable tools to optimize their PBI membrane for their application and requirements.

CRediT authorship contribution statement

Elizabeth Hampson: Writing – review & editing, Writing – original draft, Visualization, Validation, Methodology, Investigation, Formal analysis, Data curation, Conceptualization. **Jacobus C. Duburg:** . **Joel Casella:** Writing – review & editing, Visualization, Validation, Methodology, Investigation, Formal analysis, Conceptualization. **Thomas J. Schmidt:** Writing – review & editing, Supervision. **Lorenz Gubler:** Writing – review & editing, Supervision, Resources, Project administration, Funding acquisition, Conceptualization.

Declaration of competing interest

The authors declare the following financial interests/personal relationships which may be considered as potential competing interests: Lorenz Gubler reports financial support was provided by Swiss National Science Foundation. If there are other authors, they declare that they have no known competing financial interests or personal relationships that could have appeared to influence the work reported in this paper.

Data availability

Data will be made available on request.

Acknowledgements

The authors gratefully acknowledge the Swiss National Science Foundation (SNSF) for providing financial support through grant number 188631 and through the Bridge Discovery scheme (grant number 176653).

Appendix A. Supplementary data

Supplementary data to this article can be found online at https://doi.org/10.1016/j.cej.2024.149930.

References

[1] E. Sánchez-Díez, E. Ventosa, M. Guarnieri, A. Trovò, C. Flox, R. Marcilla, F. Soavi, P. Mazur, E. Aranzabe, R. Ferret, Redox flow batteries: status and perspective towards sustainable stationary energy storage, J. Power Sources 481 (2021) 228804, https://doi.org/10.1016/j.jpowsour.2020.228804.
[2] Z. Huang, A. Mu, L. Wu, B. Yang, Y. Qian, J. Wang, Comprehensive analysis of critical issues in all-vanadium redox flow battery, ACS Sustain. Chem. Eng. 10 (24) (2022) 7786–7810, https://doi.org/10.1021/acssuschemeng.2c01372.
[3] C. Minke, T. Turek, Economics of vanadium redox flow battery membranes, J. Power Sources 286 (2015) 247–257, https://doi.org/10.1016/j.jpowsour.2015.03.144.
[4] L. Tang, P. Leung, M.R. Mohamed, Q. Xu, S. Dai, X. Zhu, C. Flox, A.A. Shah, Q. Liao, Capital cost evaluation of conventional and emerging redox flow batteries for grid storage applications, Electrochim. Acta 437 (2023) 141460, https://doi.org/10.1016/j.electacta.2022.141460.
[5] L. Gubler, Membranes and separators for redox flow batteries, Curr. Opin. Electrochem. 18 (2019) 31–36, https://doi.org/10.1016/j.coelec.2019.08.007.
[6] B. Jiang, L. Yu, L. Wu, D. Mu, L. Liu, J. Xi, X. Qiu, Insights into the impact of the nafion membrane pretreatment process on vanadium flow battery performance, ACS Appl. Mater. Interfaces 8 (19) (2016) 12228–12238, https://doi.org/10.1021/acsami.6b03529.
[7] C.H.L. Tempelman, J.F. Jacobs, R.M. Balzer, V. Degirmenci, Membranes for all vanadium redox flow batteries, J. Storage Mater. 32 (2020) 101754, https://doi.org/10.1016/j.est.2020.101754.
[8] C. Minke, U. Kunz, T. Turek, Techno-economic assessment of novel vanadium redox flow batteries with large-area cells, J. Power Sources 361 (2017) 105–114, https://doi.org/10.1016/j.jpowsour.2017.06.066.
[9] J. Ye, D. Yuan, M. Ding, Y. Long, T. Long, L. Sun, C. Jia, A cost-effective nafion/lignin composite membrane with low vanadium ion permeation for high performance vanadium redox flow battery, J. Power Sources 482 (2021) 229023, https://doi.org/10.1016/j.jpowsour.2020.229023.
[10] M. Feng, R. Qu, Z. Wei, L. Wang, P. Sun, Z. Wang, Characterization of the thermolysis products of nafion membrane: a potential source of perfluorinated compounds in the environment, Sci. Rep. 5 (1) (2015) 9859, https://doi.org/10.1038/srep09859.
[11] European Commission SWD, Poly- and Perfluoroalkyl Substances (PFAS), 2020. https://eur-lex.europa.eu/legal-content/EN/ALL/?uri=SWD:2020:249:FIN. (Accessed 2023 13 March).
[12] K.E. Rodby, T.J. Carney, Y. Ashraf Gandomi, J.L. Barton, R.M. Darling, F. R. Brushett, Assessing the levelized cost of vanadium redox flow batteries with capacity fade and rebalancing, J. Power Sources 460 (2020) 227958, https://doi.org/10.1016/j.jpowsour.2020.227958.
[13] N. Poli, M. Schäffer, A. Trovò, J. Noack, M. Guarnieri, P. Fischer, Novel electrolyte rebalancing method for vanadium redox flow batteries, Chem. Eng. J. 405 (2021) 126583, https://doi.org/10.1016/j.cej.2020.126583.
[14] Z. Yuan, Y. Duan, H. Zhang, X. Li, H. Zhang, I. Vankelecom, Advanced porous membranes with ultra-high selectivity and stability for vanadium flow batteries, Energ. Environ. Sci. 9 (2) (2016) 441–447, https://doi.org/10.1039/C5EE02896E.
[15] D. Aili, J. Yang, K. Jankova, D. Henkensmeier, Q. Li, From polybenzimidazoles to polybenzimidazoliums and polybenzimidazolides, J. Mater. Chem. A 8 (26) (2020) 12854–12886, https://doi.org/10.1039/D0TA01788D.
[16] S.-Y. Choi, S. Cho, D. Kim, J. Kim, G. Song, R. Singh, C. Kim, Boosting the proton conduction using protonated imidazole for advanced ion conducting membrane, J. Membr. Sci. 620 (2021) 118904, https://doi.org/10.1016/j.memsci.2020.118904.

[17] L. Zeng, T.S. Zhao, L. Wei, H.R. Jiang, M.C. Wu, Anion exchange membranes for aqueous acid-based redox flow batteries: current status and challenges, Appl. Energy 233–234 (2019) 622–643, https://doi.org/10.1016/j.apenergy.2018.10.063.
[18] X. Yan, Z. Dong, M. Di, L. Hu, C. Zhang, Y. Pan, N. Zhang, X. Jiang, X. Wu, J. Wang, G. He, A highly proton-conductive and vanadium-rejected long-side-chain sulfonated polybenzimidazole membrane for redox flow battery, J. Membr. Sci. 596 (2020) 117616, https://doi.org/10.1016/j.memsci.2019.117616.
[19] L. Wang, A.T. Pingitore, W. Xie, Z. Yang, M.L. Perry, B.C. Benicewicz, Sulfonated PBI gel membranes for redox flow batteries, J. Electrochem. Soc. 166 (8) (2019) A1449, https://doi.org/10.1149/2.0471908jes.
[20] Y.H. Wan, J. Sun, Q.P. Jian, X.Z. Fan, T.S. Zhao, A nafion/polybenzimidazole composite membrane with consecutive proton-conducting pathways for aqueous redox flow batteries, J. Mater. Chem. A 10 (24) (2022) 13021–13030, https://doi.org/10.1039/D2TA01746F.
[21] J.C. Duburg, K. Azizi, S. Primdahl, H.A. Hjuler, E. Zanzola, T.J. Schmidt, L. Gubler, Composite polybenzimidazole membrane with high capacity retention for vanadium redox flow batteries, Molecules 26 (6) (2021) 1679.
[22] Y.H. Wan, J. Sun, H.R. Jiang, X.Z. Fan, T.S. Zhao, A highly-efficient composite polybenzimidazole membrane for vanadium redox flow battery, J. Power Sources 489 (2021) 229502, https://doi.org/10.1016/j.jpowsour.2021.229502.
[23] M. Shi, Q. Dai, F. Li, T. Li, G. Hou, H. Zhang, X. Li, Membranes with well-defined selective layer regulated by controlled solvent diffusion for high power density flow battery, Adv. Energy Mater. 10 (34) (2020) 2001382, https://doi.org/10.1002/aenm.202001382.
[24] L. Qiao, H. Zhang, W. Lu, Q. Dai, X. Li, Advanced porous membranes with tunable morphology regulated by ionic strength of nonsolvent for flow battery, ACS Appl. Mater. Interfaces 11 (27) (2019) 24107–24113, https://doi.org/10.1021/acsami.9b06142.
[25] M. Mara Ikhsan, S. Abbas, X.H. Do, S.-Y. Choi, K. Azizi, H.A. Hjuler, J.H. Jang, H. Y. Ha, D. Henkensmeier, Polybenzimidazole membranes for vanadium redox flow batteries: effect of sulfuric acid doping conditions, Chem. Eng. J. 435 (2022) 134902, https://doi.org/10.1016/j.cej.2022.134902.
[26] S. Peng, X. Yan, D. Zhang, X. Wu, Y. Luo, G. He, A H3PO4 preswelling strategy to enhance the proton conductivity of a H2SO4-doped polybenzimidazole membrane for vanadium flow batteries, RSC Adv. 6 (28) (2016) 23479–23488, https://doi.org/10.1039/C6RA00831C.
[27] B. Xing, O. Savadogo, Hydrogen/oxygen polymer electrolyte membrane fuel cells (PEMFCs) based on alkaline-doped polybenzimidazole (PBI), Electrochem. Commun. 2 (10) (2000) 697–702, https://doi.org/10.1016/S1388-2481(00)00107-7.
[28] H. Hou, G. Sun, R. He, Z. Wu, B. Sun, Alkali doped polybenzimidazole membrane for high performance alkaline direct ethanol fuel cell, J. Power Sources 182 (1) (2008) 95–99, https://doi.org/10.1016/j.jpowsour.2008.04.010.
[29] D. Aili, K. Jankova, J. Han, N.J. Bjerrum, J.O. Jensen, Q. Li, Understanding ternary poly(potassium benzimidazolide)-based polymer electrolytes, Polymer 84 (2016) 304–310, https://doi.org/10.1016/j.polymer.2016.01.011.
[30] D. Aili, K. Jankova, Q. Li, N.J. Bjerrum, J.O. Jensen, The stability of poly(2,2′-(m-phenylene)-5,5′-bibenzimidazole) membranes in aqueous potassium hydroxide, J. Membr. Sci. 492 (2015) 422–429, https://doi.org/10.1016/j.memsci.2015.06.001.
[31] C. Noh, D. Serhiichuk, N. Malikah, Y. Kwon, D. Henkensmeier, Optimizing the performance of meta-polybenzimidazole membranes in vanadium redox flow batteries by adding an alkaline pre-swelling step, Chem. Eng. J. 407 (2021) 126574, https://doi.org/10.1016/j.cej.2020.126574.
[32] E. Babcock, N. Szekely, A. Konovalova, Y. Lin, M.S. Appavou, G. Mangiapia, Z. Revay, C. Stieghorst, O. Holderer, D. Henkensmeier, W. Lehnert, M. Carmo, Using neutron methods SANS and PGAA to study evolution of structure and composition of alkali-doped polybenzimidazole membranes, J. Membr. Sci. 577 (2019) 12–19, https://doi.org/10.1016/j.memsci.2019.01.026.
[33] M.L.A. Trisno, A. Dayan, S.J. Lee, F. Egert, M. Gerle, M.R. Kraglund, J.O. Jensen, D. Aili, A. Roznowska, A. Michalak, H.S. Park, F. Razmjooei, S.-A. Ansar, D. Henkensmeier, Reinforced gel-state polybenzimidazole hydrogen separators for alkaline water electrolysis, Energ. Environ. Sci. 15 (10) (2022) 4362–4375, https://doi.org/10.1039/D2EE01922A.
[34] M.R. Kraglund, D. Aili, K. Jankova, E. Christensen, Q. Li, J.O. Jensen, Zero-gap alkaline water electrolysis using ion-solvating polymer electrolyte membranes at reduced KOH concentrations, J. Electrochem. Soc. 163 (11) (2016) F3125, https://doi.org/10.1149/2.0161611jes.
[35] D. Aili, M.K. Hansen, R.F. Renzaho, Q. Li, E. Christensen, J.O. Jensen, N.J. Bjerrum, Heterogeneous anion conducting membranes based on linear and crosslinked KOH doped polybenzimidazole for alkaline water electrolysis, J. Membr. Sci. 447 (2013) 424–432, https://doi.org/10.1016/j.memsci.2013.07.054.
[36] T. Patniboon, H.A. Hansen, Degradation of polybenzimidazole in alkaline solution with first-principles modeling, Electrochim. Acta 398 (2021) 139329, https://doi.org/10.1016/j.electacta.2021.139329.
[37] X. Wu, X. Wang, G. He, J. Benziger, Differences in water sorption and proton conductivity between nafion and SPEEK, J Polym Sci B 49 (20) (2011) 1437–1445, https://doi.org/10.1002/polb.22326.
[38] Q. Li, R. He, R.W. Berg, H.A. Hjuler, N.J. Bjerrum, Water uptake and acid doping of polybenzimidazoles as electrolyte membranes for fuel cells, Solid State Ion. 168 (1) (2004) 177–185, https://doi.org/10.1016/j.ssi.2004.02.013.
[39] J. Chen, J. Cao, R. Zhang, J. Zhou, S. Wang, X. Liu, T. Zhang, X. Tao, Y. Zhang, Modifications on promoting the proton conductivity of polybenzimidazole-based polymer electrolyte membranes in fuel cells, Membranes 11 (11) (2021) 826, https://doi.org/10.3390/membranes11110826.
[40] F.J. Oldenburg, T.J. Schmidt, L. Gubler, Tackling capacity fading in vanadium flow batteries with amphoteric membranes, J. Power Sources 368 (2017) 68–72, https://doi.org/10.1016/j.jpowsour.2017.09.051.
[41] O. Nibel, T.J. Schmidt, L. Gubler, Bifunctional ion-conducting polymer electrolyte for the vanadium redox flow battery with high selectivity, J. Electrochem. Soc. 163 (13) (2016) A2563–A2570, https://doi.org/10.1149/2.0441613jes.
[42] C. Noh, M. Jung, D. Henkensmeier, S.W. Nam, Y. Kwon, Vanadium redox flow batteries using meta-polybenzimidazole-based membranes of different thicknesses, ACS Appl. Mater. Interfaces 9 (42) (2017) 36799–36809, https://doi.org/10.1021/acsami.7b10598.
[43] F.J. Oldenburg, E. Nilsson, T.J. Schmidt, L. Gubler, Tackling capacity fading in vanadium redox flow batteries with amphoteric polybenzimidazole/nafion bilayer membranes, Chem. Sus. Chem 12 (12) (2019) 2620–2627, https://doi.org/10.1002/cssc.201900546.
[44] P. Xiong, L. Zhang, Y. Chen, S. Peng, G. Yu, A chemistry and microstructure perspective on ion-conducting membranes for redox flow batteries, Angew. Chem. Int. Ed. 60 (47) (2021) 24770–24798, https://doi.org/10.1002/anie.202105619.
[45] T. Okada, G. Xie, O. Gorseth, S. Kjelstrup, N. Nakamura, T. Arimura, Ion and water transport characteristics of Nafion membranes as electrolytes, Electrochimica Acta 43 (24) (1998) 3741–3747, https://doi.org/10.1016/S0013-4686(98)00132-7.
[46] J. Hu, H. Zhang, W. Xu, Z. Yuan, X. Li, Mechanism and transfer behavior of ions in Nafion membranes under alkaline media, Journal of Membrane Science 566 (2018) 8–14, https://doi.org/10.1016/j.memsci.2018.08.057.